

Gating of human ClC-2 chloride channels and regulation by carboxy-terminal domains

Jennie Garcia-Olivares¹, Alexi Alekov¹, Mohammad Reza Boroumand¹, Birgit Begemann¹, Patricia Hidalgo¹ and Christoph Fahlke^{1,2}

¹Institut für Neurophysiologie, Medizinische Hochschule Hannover, ²Zentrum für Systemische Neurowissenschaften Hannover (ZSN), Germany

Eukaryotic ClC channels are dimeric proteins with each subunit forming an individual protopore. Single protopores are gated by a fast gate, whereas the slow gate is assumed to control both protopores through a cooperative movement of the two carboxy-terminal domains. We here study the role of the carboxy-terminal domain in modulating fast and slow gating of human ClC-2 channels, a ubiquitously expressed ClC-type chloride channel involved in transepithelial solute transport and in neuronal chloride homeostasis. Partial truncation of the carboxy-terminus abolishes function of ClC-2 by locking the channel in a closed position. However, unlike other isoforms, its complete removal preserves function of ClC-2. ClC-2 channels without the carboxy-terminus exhibit fast and slow gates that activate and deactivate significantly faster than in WT channels. In contrast to the prevalent view, a single carboxy-terminus suffices for normal slow gating, whereas both domains regulate fast gating of individual protopores. Our findings demonstrate that the carboxy-terminus is not strictly required for slow gating and that the cooperative gating resides in other regions of the channel protein. ClC-2 is expressed in neurons and believed to open at negative potentials and increased internal chloride concentrations after intense synaptic activity. We propose that the function of the ClC-2 carboxy-terminus is to slow down the time course of channel activation in order to stabilize neuronal excitability

(Received 10 June 2008; accepted after revision 16 September 2008; first published online 18 September 2008)

Corresponding author Ch. Fahlke: Institut für Neurophysiologie, Medizinische Hochschule Hannover, Carl-Neuberg-Str. 1, 30625 Hannover, Germany. Email: fahlke.christoph@mh-hannover.de

ClC channels and transporters are present in almost all prokaryotic and eukaryotic cells (Jentsch *et al.* 2002). Eukaryotic isoforms exhibit large cytoplasmic carboxy-termini that fulfil multiple isoform-specific functions. The carboxy-terminus of intracellular ClC transporters is involved in intracellular trafficking and function (Schwappach *et al.* 1998; Carr *et al.* 2003; Mo *et al.* 2004). Carboxy-terminal truncations abolish macroscopic currents of ClC-0 and ClC-1 (Hryciw *et al.* 1998; Maduke *et al.* 1998; Estevez *et al.* 2004; Wu *et al.* 2006) by preventing surface insertion (Maduke *et al.* 1998; Estevez *et al.* 2004) or by permanently closing the mutant channel (Hebeisen *et al.* 2004).

ClC-0 and ClC-1 channels are activated by membrane depolarization and increased extracellular chloride concentrations (Pusch *et al.* 1995; Chen & Miller, 1996; Rychkov *et al.* 1996). Mutations and deletions within the carboxy-terminus shift the voltage dependence of activation (Beck *et al.* 1996) by modifying anion binding to

the external pore vestibule (Hebeisen & Fahlke, 2005). For ClC-0 and ClC-1, it has been proposed that the association between the carboxy-termini of each subunit underlies the concerted opening and closing of the two protopores – the so-called slow or common gating (Fong *et al.* 1998; Estevez *et al.* 2004; Bykova *et al.* 2006).

High resolution structures of the carboxy-termini are now available for three isoforms, ClC-0, ClC-5 and ClC-Ka (Meyer & Dutzler, 2006; Markovic & Dutzler, 2007; Meyer *et al.* 2007). These structures revealed a conserved pair of tightly interacting CBS motifs connected by a variable linker and followed by an unstructured distal end. The CBS1–CBS2 linker consists of a flexible region and an α -helical region preceding CBS2. Although tight binding of CBS1 and CBS2 is a general feature of ClC carboxy-termini, CBS–CBS interactions are not necessary for certain functions of the carboxy-terminus. For ClC-1, the presence of only one CBS domain is sufficient for normal function and trafficking of ClC-1 (Estevez *et al.* 2004; Hebeisen *et al.* 2004).

We here focused on human ClC-2, a ClC-type chloride channel involved in transepithelial solute

This paper has online supplemental material.

transport (Catalan *et al.* 2004) and in intracellular neuronal $[\text{Cl}^-]$ homeostasis (Haug *et al.* 2003). ClC-2 differs from ClC-0 and ClC-1 in the voltage dependence of gating. ClC-2 is activated by membrane hyperpolarization and intracellular anions (Thiemann *et al.* 1992; Park *et al.* 1998; Haug *et al.* 2003; Niemeyer *et al.* 2003; de Santiago *et al.* 2005). We demonstrate that ClC-2 is functional even in the complete absence of its carboxy-terminal domain ($\text{CT}_{\text{hClC-2}}$), whereas the presence of only one CBS domain locks the channel in a closed conformation. Removal of the carboxy-terminus abolishes neither fast nor slow gating, but accelerates activation and deactivation of both processes.

Methods

Construction of expression plasmids, mutagenesis and heterologous expression

The coding region of hClC-2 (Swiss-Prot entry: P51788, kindly provided by Dr G. Cutting, Johns Hopkins University; Baltimore, MD, USA) (Cid *et al.* 1995) was subcloned into pRcCMV. Two mutations, Y17H and R210H, were inserted, based on a comparison with DNA sequences of 360 control chromosomes (Haug *et al.* 2003), and the corrected coding region was then subcloned into pSVL or pcDNA5FTR/TO. Different mutations (truncation, deletion, insertion and point mutation) were introduced into the plasmid pRcCMV-hClC-2 or pSVL-hClC-2 by PCR-based strategies. Construction of concatamers was performed as previously described (Fahlke *et al.* 1997; Haug *et al.* 2003). All mutations were verified by DNA sequencing, and two independent mutant clones were tested, yielding identical results.

Transient transfections in tsA201 cells were performed with 3–10 μg of plasmid DNA using a calcium phosphate precipitation method as described (Melzer *et al.* 2005). A stable inducible cell line, generated by selecting Flp-In-T-Rex 293 cells (Invitrogen) transfected with pcDNA5/FRT/TO-hClC-2, was used 2 h after incubation with 0.2 $\mu\text{g ml}^{-1}$ tetracycline. Co-expression of complementary regions was performed using yellow fluorescent protein (YFP) and cyan fluorescent protein (CFP) fusion proteins and only cells containing both fluorescent signals were analysed.

Confocal microscopy and surface expression assay

Cell imaging was carried out in MDCK and tsA201 cells expressing fusion proteins of hClC-2 with monomeric YFP (mYFP-hClC-2) using a Leica DM IRB confocal microscope with a TCS SP2 AOBS scan head. For immuno-surface labelling, a haemagglutinin (HA) tag was inserted into the extracellular loop between helices

L and M of mYFP-hClC-2 channel at amino acid position 416 by standard overlapping PCR. Cells were allowed to grow on a glass coverslip and fixed for 20 min with 4% paraformaldehyde. Fixed cells were blocked with phosphate saline buffer containing 1% BSA, incubated with anti-HA antibody (3F10, Roche), washed four times, and incubated with antirat IgG antibody conjugated with Alexa 488 (Molecular Probes).

To quantify membrane surface insertion, intact tsA201 cells were incubated on ice for 1 h with anti-HA antibody (3F10, Roche Applied Science) and chemically lysed with 100 mM phosphate buffer, 150 mM NaCl, and 1% NP-40 supplemented with complete inhibitor protease cocktail (Roche Applied Science). One microlitre of cell lysate was blotted onto HybondECL membrane (GE Healthcare Life Sciences). The membrane was blocked with phosphate saline buffer containing 3% BSA, and subsequently washed and incubated with a secondary antibody conjugated to Alexa 546 (Molecular Probes). Two consecutive laser scanings (Typhoon 9400, GE Healthcare Life Sciences) were used to detect the two fluorescence signals. The signal intensity (quantified with ImageQuant software (GE Healthcare Life Science)) of YFP fluorescence (F_{YFP}) was taken as the total amount of expressed channels and of Alexa 546 (F_{546}) as the amount of channels expressed at the plasma membrane. The relative amount of surface channels $R_{\text{Surface/Total}}$ was calculated as the ratio of the F_{YFP} (Total channels) and F_{546} (surface channels) of treated cells with anti-HA antibody after subtraction of a ratio F_{546}/F_{YFP} of cells not treated with anti-HA antibody.

$$R_{\text{Surface/Total}} = \left[\frac{F_{546}}{F_{\text{YFP}}} \right]_{\text{Treated}} - \left[\frac{F_{546}}{F_{\text{YFP}}} \right]_{\text{Non-treated}} \quad (1)$$

Electrophysiology and data analysis

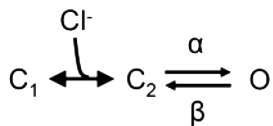
Standard whole-cell patch clamp recordings were performed as previously described (Hebeisen *et al.* 2003). The standard extracellular solution contained (in mM): NaCl (140), KCl (4), CaCl_2 (2), MgCl_2 (1), Hepes (5); the standard intracellular solution contained (in mM): NaCl (115), MgCl_2 (2), EGTA (5), Hepes (10). All solutions were adjusted to pH 7.4. The cells were clamped to 0 mV between test sweeps.

Data were analysed by pCLAMP (Molecular Devices; Sunnyvale, CA, USA) and SigmaPlot (Systat Software Inc., San Jose, CA, USA). To obtain the voltage dependence of the relative open probability, instantaneous current amplitudes were determined 200 μs after a voltage step to -100 mV following prepulses to various voltages, normalized by their maximum value and plotted against the preceding potential. The durations of the prepulses were adjusted to allow steady-state activation. To determine the voltage dependence of the opening of the

slow gate, a short (3–5 ms) pulse to -200 mV was inserted before the test step to -100 mV to fully activate the fast gate at this potential. The duration of the -200 mV pulse was set to twice the fast activation time constant at this potential. The relative open probabilities of the fast gate (P_f) were calculated by dividing the voltage dependence of the relative open probability (P_o) by the open probability of the slow gate (P_s). The voltage dependences of absolute open probabilities (P_{abs}), relative open probabilities at different voltages, were normalized to the maximum absolute open probability obtained by noise analysis.

We used a modification of the Chen–Miller model (Chen & Miller, 1996) to further describe gating of WT and mutant ClC-2. This model was introduced for fast gating of ClC-0 and subsequently shown to describe fast and slow gating of ClC-1 (Duffield *et al.* 2003; Hebeisen & Fahlke, 2005). For these two isoforms, the opening rate constants increase at negative and positive potentials, caused by the existence of two open states, one linked to a voltage-dependent translocation of a Cl^- ion (Chen & Miller, 1996; Hebeisen & Fahlke, 2005), the other one most likely linked to a pH-dependent opening transition that is stimulated by negative membrane potentials (Chen & Chen, 2001). Whereas translocation of extracellular Cl^- confers the voltage dependence of ClC-0 and ClC-1 (Pusch *et al.* 1995; Rychkov *et al.* 1996; Chen & Miller, 1996; Hebeisen & Fahlke, 2005), ClC-2 channels are gated by intracellular Cl^- (Haug *et al.* 2003). In mouse ClC-2, membrane hyperpolarization promotes the entering into chloride-activated and proton-activated (Arreola *et al.* 2002) open states.

Under the simplifying assumption that fast and slow gating are independent, gating of the fast and slow gates of hClC-2 can be described with a modification of the Chen–Miller model that removes one open state and lumps together the inward movement of the bound Cl^- and the subsequent channel opening step:



In this gating scheme, an anion binding site is accessible in the closed state, and closed states with and without bound anion are in rapid equilibrium. At high intracellular $[\text{Cl}^-]$, gating of the fast and slow gate can be adequately described by a two-state diagram. This analysis enables determination of opening and closing rate constants and the effect of carboxy-terminal truncations on these values. It is sufficient to describe all our experimental results.

Opening rates (α) of the fast and slow gates were calculated according to:

$$\alpha_{f,s} = P_{f,s}/\tau$$

We are only able to determine the absolute probability of channel opening ($P_{open} = P_f P_s$), but not individual absolute open probabilities of the fast or the slow gate. The maximum open probabilities of WT and mutant channels are around 0.75, indicating that the maximum values of P_f and P_s are between 0.75 and 1. We assumed that the maximum values of the fast and slow gate open probabilities are the same. Closing rates ($\beta_{f,s} = 1 - P_{f,s}/\tau$) were only determined at positive potentials, when all tested channels exhibit $P_f = 0$. The voltage dependencies of opening and closing rate constants were fitted with $\alpha(V) = \alpha(-155 \text{ mV} / +115 \text{ mV}) e^{ze_0 V/kT}$ (Table 1), with V being the membrane potential, e_0 the elementary charge, T the absolute temperature and k the Boltzmann constant.

All values are given as means \pm S.E.M.

Noise analysis

Current variances and mean current amplitudes were determined during the last 100 ms of a 1 s test step to voltages between -155 and $+45$ mV. Current traces were sampled at 200 kHz and filtered using a Butterworth low pass filter with a cutoff frequency of 10 kHz. The variance at the current reversal potential was subtracted as background noise. For all experiments, the analysis was repeated after digital filtering at 5 kHz and at 2 kHz with similar results.

Lorentzian noise depends on the number of channels (N), the unitary current amplitude (i), and the absolute open probability (p), as:

$$\sigma^2 = Ni^2 p(1 - p) \quad (2)$$

or:

$$\frac{\sigma^2}{I} = i(1 - p) = i - \frac{I}{N} \quad (3)$$

We employed a variation of stationary variance analysis (Sesti & Goldstein, 1998; Torres-Salazar & Fahlke, 2007). hClC-2 channels exhibit a voltage-independent unitary conductance (γ), and dividing both sides by $V - V_r$, with V_r being the reversal potential, results in:

$$\frac{\sigma^2}{I(V - V_r)} = \frac{i}{V - V_r} - \frac{I}{(V - V_r)N} = \gamma - \frac{I}{(V - V_r)N} \quad (4)$$

Plotting the variance divided by the product of the current amplitude and $V - V_r$ against the macroscopic conductance results in a linear relationship, with γ as the y -axis intercept and $1/N$ as the slope. The single channel amplitude (i) and the absolute open probability (p) were then calculated as $i = \gamma(V - V_r)$ and $p = I/Ni$.

Results

Functional consequences of carboxy-terminal truncations of hClC-2

Based on the known structures of mammalian carboxy-termini and limited proteolysis analysis on CT_{hClC-2} (data not shown), three truncation mutants (H573X, removing the whole CT_{hClC-2}; R751X, removing half of CT_{hClC-2}, and V872X, removing the region distal to CBS2) and two deletions, one removing CBS1 (Δ (H573–L636)) and another one deleting CBS2 plus the preceding α -helix (Δ (G730–H840)) were designed, expressed in tsA201 cells, and studied through whole-cell patch clamping (Fig. 1A). Cells expressing R751X, Δ (H573–L636) or Δ (G730–H840) hClC-2 did not exhibit anion currents (Fig. 1A). In contrast, H573X or V872X truncated channels resulted in macroscopic current amplitudes comparable to those of WT hClC-2 (Fig. 1A).

hClC-2 thus tolerates the complete removal of its carboxy-terminus (H573X). Isolated CBS domains (R751X, Δ (H573–L636) and Δ (G730–H840)) exert an inhibitory effect on hClC-2 channels. This inhibition can be relieved by the complementary CBS domain in WT or V872X hClC-2. However, this rescue relies on additional interactions within the carboxy-terminus. Co-transfecting complementary carboxy-terminal peptides does not restore channel function of R751X hClC-2 (Fig. 1B), in clear contrast to other ClC isoforms (Hebeisen *et al.* 2004;

Hryciw *et al.* 1998; Maduke *et al.* 1998; Estevez *et al.* 2004; Mo *et al.* 2004).

Figure 1B shows representative current recordings from WT, V872X and H573X hClC-2. WT hClC-2 is closed at positive potentials and slowly activates on a biexponential time course upon hyperpolarizing voltage steps (Cid *et al.* 1995; Haug *et al.* 2003). Stepping back to a positive potential results in channel deactivation. Deleting the fragment distal to CBS2 (V872X) or the complete carboxy-terminus causes a pronounced acceleration of the time course of activation and deactivation (Fig. 1B).

Our results demonstrate that CT_{hClC-2} regulates kinetics of channel gating and that normal function of hClC-2 relies on interactions within the carboxy-terminus.

CT_{hClC-2} is not required for channel surface membrane insertion

The absence of macroscopic current amplitudes might be due to an insufficient transcription/translation, a lack of surface membrane insertion, or the loss of function of truncated channels. We first tested the production of mutant hClC-2 by expressing fusion proteins of WT and mutant hClC-2 covalently linked to yellow fluorescent protein (YFP) in tsA201 cells and analysing them by SDS-PAGE. YFP fluorescence intensities were comparable for WT and truncated channels (data not shown), indicating that carboxy-terminal truncations do not reduce expression levels of hClC-2.

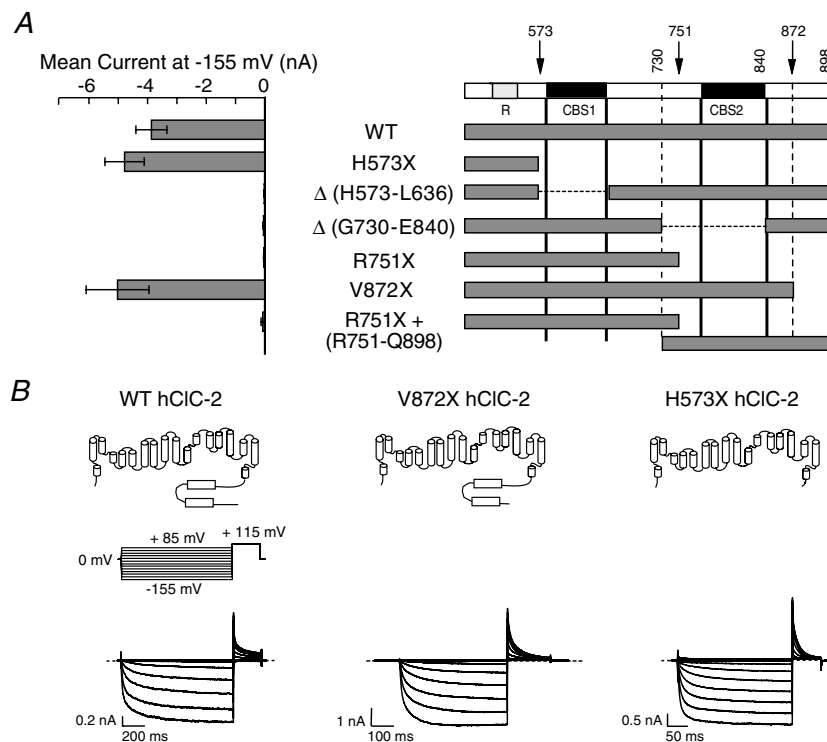


Figure 1. Deletions of different regions within the carboxy-terminus have distinct effect on channel function

A, steady-state mean current amplitudes at -155 mV ($8 < n > 21$) measured in cells expressing WT and mutant hClC-2 channels (left panel) and schematic representation of the corresponding channel construct used in this study (right panel). The numbers denote the amino acid residue position in the WT hClC-2 channel sequence. Deletions (Δ) are represented as a dashed line. **B**, schematic depictions, pulse protocol and representative current traces of WT, H573X and V872X hClC-2 channels expressed in tsA201 cells.

To assess whether carboxy-terminal truncations affect intracellular trafficking, we studied surface expression of WT, R751X, and H573X hClC-2, using confocal imaging, immunohistochemistry and immunoassays. Confocal imaging of cells expressing the non-functional channel mYFP-R751X hClC-2 shows a subcellular distribution comparable with mYFP-WT channel (Fig. 2A). Immunohistochemistry using a haemagglutinin (HA) tag incorporated into an extracellular channel loop under non-permeable conditions shows a clear membrane staining of WT and R751X hClC-2-HA (Fig. 2A). To quantify the relative amount of hClC-2 channels in the surface membrane, we created doubly tagged hClC-2 with an amino-terminal mYFP and the HA tag in the extracellular loop. Since each hClC-2 is linked to the mYFP moiety, mYFP fluorescence intensities are proportional to total numbers of channels. In contrast, the HA tag is only accessible from the outside under non-permeable cellular conditions, allowing quantification of the number of hClC-2 channels in the surface membrane by immuno-

reaction with an antibody coupled to the fluorescent dye Alexa 546. We calculated the relative amount of channels present in the plasma membrane as the ratio of Alexa 546 and YFP fluorescence intensities of anti-HA treated cells. This analysis demonstrates that surface membrane insertion of R751X and H573X channels is comparable to WT channels (Fig. 2B). In contrast, S551X that lacks the transmembrane R helix and the complete carboxy-terminal domain results in intracellular retention of mutant channels. We conclude that the carboxy-terminus is not necessary for surface membrane insertion of hClC-2.

R751X constitutively locks the channel in a closed conformation

Since truncated channels are inserted into the surface membrane at similar percentages as WT hClC-2, the loss of function must originate from permanent closure of truncated channels. To test this hypothesis, we

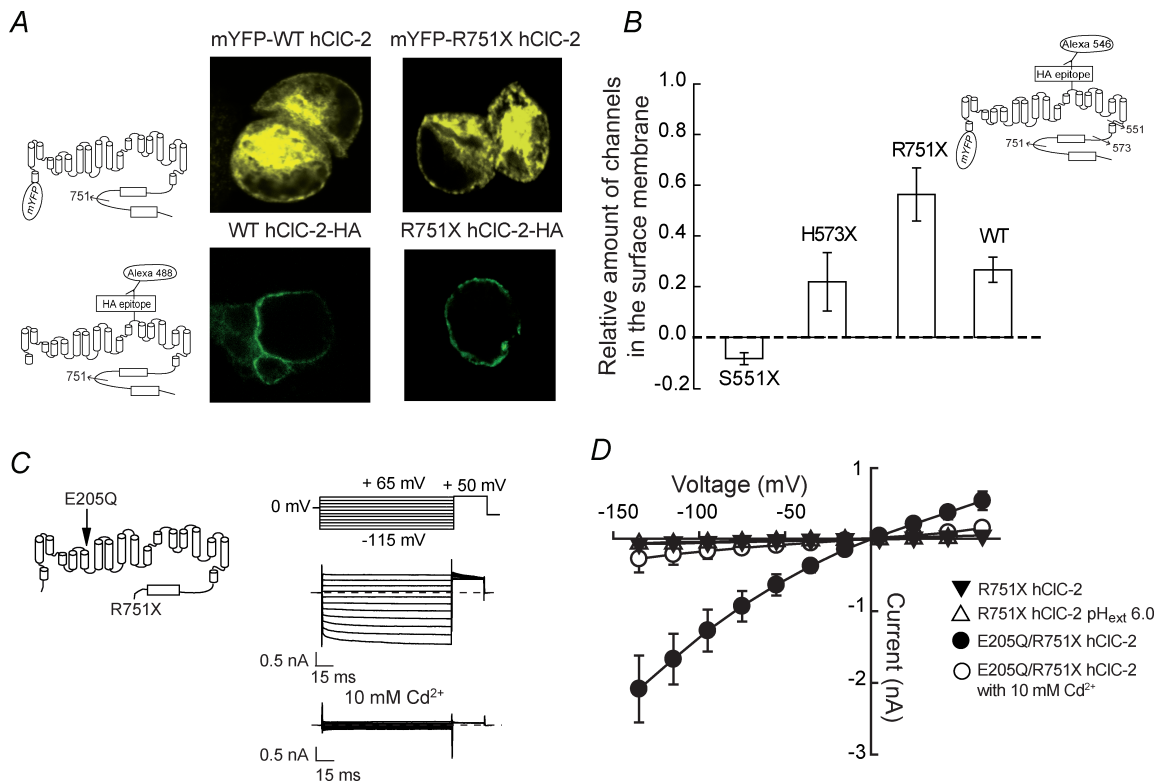


Figure 2. Effects of carboxy-terminal truncations on channel activity and surface expression

A, schematic depictions of channel constructs used and confocal images of cells expressing WT hClC-2 or R751X hClC-2 channels fused to either mYFP (upper) or HA epitope tagged after immunodetection with Alexa 488-conjugated antibody (lower). B, bar plot of the relative amount of channels expressed at the plasma membrane (average of 4 separate experiments) and schematic depictions of the construct used. C, neutralization of the protopore gate (E205Q) recovers the function of truncated R751X hClC-2. Pulse protocol and representative current recordings of tsA201 cells expressing E205Q/R751X hClC-2 channels, before and after the application of 10 mM Cd²⁺. D, current-voltage relationships for R751X hClC-2 (n = 15), R751X hClC-2 in external pH 6 (n = 8), and E205Q/R751X hClC-2 before (n = 6) and after (n = 4) applying 10 mM Cd²⁺.

incorporated a charge-neutralizing mutation at position 205 (E205Q) (Dutzler *et al.* 2003) – located in the F helix of the transmembrane core – into the R751X truncated channel (Fig. 2C). The corresponding substitution in full length mouse and rat ClC2 keeps the fast gate permanently open and abolishes a significant fraction of the slow gating (Niemeyer *et al.* 2003; de Santiago *et al.* 2005).

Cells expressing E205Q/R751X hClC-2 channels display anion currents over the whole voltage range that further activate upon hyperpolarizing voltage steps down to -60 mV (Fig. 2C). These currents are conducted by hClC-2 channels, as supported by the fact that 10 mM of Cd^{2+} results in a fast and complete current block (Fig. 2C and D). Hence, E205Q does restore the functioning of R751X hClC-2 channels, indicating that R751X abolishes channel function by locking the channel in a closed conformation. External acidification was also reported to activate ClC-2 (Arreola *et al.* 2002). However, R751X hClC-2 is not functional at an external pH of 6.0 (Fig. 2D).

CT_{hClC-2} decelerates activation and deactivation in hClC-2 channels

To study how the intact carboxy-terminus decelerates hClC-2 gating, we compared the gating of WT and H573X hClC-2. We first employed a modification of stationary noise analysis (Sesti & Goldstein, 1998) to determine absolute open probabilities of WT and mutant hClC-2 (Fig. 3). In contrast to conventional non-stationary noise analysis that is based on time-dependent changes of the channels' open probability (Sigworth, 1980), we analysed

steady-state mean current amplitudes (I) and current variances (σ^2) at various voltages between -155 and $+45$ mV. This approach does not require large numbers of identical voltage steps and is thus ideally suited for channels with slow gating kinetics.

Since ClC-2 exhibits a constant conductance γ , a plot of the variances divided by the product of the mean current amplitudes and the electrical driving force ($V - V_r$) against the macroscopic conductance (Fig. 3A and B) allows determination of unitary channel properties by a linear fit (see eqn (4) in Methods). The slope ($-1/N$) of the fitted straight gives the number of channels (N), and the y -axis intercept provides the unitary conductance (γ). Using this approach, we determined unitary current amplitudes for H573X and WT hClC-2. Truncations do not affect the single channel amplitude (-0.38 ± 0.06 pA at -155 mV, $n = 6$, for WT and -0.35 ± 0.10 pA, $n = 4$, for H573X hClC-2). Our estimates of unitary current amplitudes of full length channels are in good agreement with single-channel recordings of rat ClC-2 (Weinreich & Jentsch, 2001; Ramjeesingh *et al.* 2006).

Maximum absolute open probabilities were calculated from macroscopic current amplitudes, single channel amplitudes and the number of channels resulting in similar values for full length and truncated channels (0.73 ± 0.02 , $n = 6$, for WT and 0.68 ± 0.01 , $n = 4$, for H573X hClC-2). To determine the voltage dependence of the relative open probability (P_o) for WT and H573X hClC-2 channels, instantaneous current amplitudes were measured at a voltage step to -100 mV after prepulses to different voltages and plotted against the preceding potential. Normalization of relative open probabilities

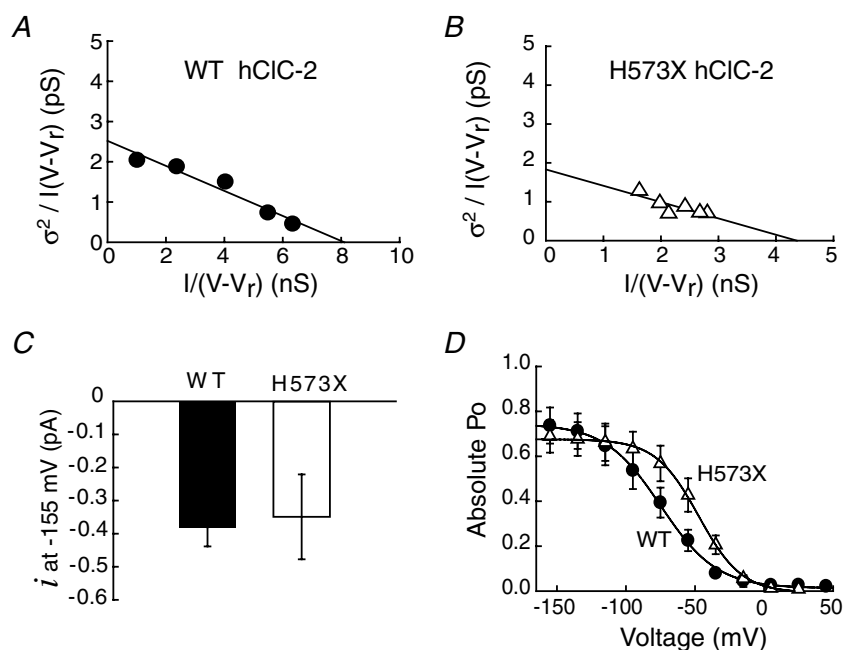


Figure 3. Stationary noise analysis of WT and H573X hClC-2

A and B, plots of the variance, normalized by the product of the mean current (I) and the electrical driving force ($V - V_r$), versus the macroscopic conductance $I/(V - V_r)$ from representative cells expressing WT (A) or H573X (B) hClC-2. C, unitary currents (i) at -155 mV of WT ($n = 6$) and H573X ($n = 4$). D, voltage dependence of the absolute open probabilities of WT ($n = 6$) and H573X ($n = 4$) channels. Fits to linear (A and B) or Boltzmann (D) functions are shown as lines.

to maximum absolute open probabilities determined by noise analysis gives the voltage dependence of the absolute open probability (Fig. 3D). H573X shifts the voltage dependence of activation to more positive potentials ($V_{1/2} = -47.7 \pm 1.0$ mV, $n = 4$, for H573X, and -74.7 ± 1.4 mV, $n = 6$, for WT).

hClC-2 displays fast openings and closings of individual protopores and slow cooperative gating steps (Zuniga *et al.* 2004; de Santiago *et al.* 2005). Assuming that fast and slow gating are independent from each other, the probability of the channel to be open (P_o) is the product of the open probabilities of both gates. To measure the relative open probability of the slow gate (P_s) in isolation, a short pulse that fully activates the fast gate was inserted prior to the test step in the voltage protocol to measure open probabilities (de Santiago *et al.* 2005) (Fig. 4A and B). The relative open probability of the fast gate (P_f) can then be calculated as the ratio of relative open probabilities of the channel to the relative slow gate open probability (Fig. 4C and D). H573X shifts the voltage dependence of the fast and the slow gate around 10 mV in the positive direction. Moreover, the minimum open probability of the slow gate is increased from 0.39 ± 0.01 ($n = 4$) in WT hClC-2 to 0.79 ± 0.01 ($n = 4$) in H573X hClC-2. WT channels activate and deactivate on a biexponential time course (Fig. 4A and E). H573X reduces the fast and slow activation and fast deactivation time constants fivefold. The increased minimum open probability of the slow gate results in a monoexponential deactivation of H573X hClC-2 at positive potentials (Fig. 4B and E).

De Santiago *et al.* (2005) recently reported that individual protopores of mouse ClC-2 activate on a biexponential time course. This finding raises the question whether the slow gating component of H573X hClC-2 might be due to slow protopore gating. To test this possibility, we studied block of WT and H573X hClC-2 by Cd^{2+} . Cd^{2+} and Zn^{2+} block ClC channels by facilitating slow deactivation (Chen, 1998), and mutations that abolish slow gating reduce the relative block by Cd^{2+} or Zn^{2+} (Lin *et al.* 1999; Zuniga *et al.* 2004). In contrast to these mutant channels, H573X hClC-2 channels are completely blocked by 1 mM Cd^{2+} (Supplementary Fig. 1), indicating that slow gating is not abolished by H573X. However, 100 μM reduces H573X hClC-2 currents to a lesser extent than WT channels, in agreement with a reduced affinity of truncated channels for Cd^{2+} .

To further quantify the effect of $\text{CT}_{\text{hClC-2}}$ on gating, we calculated apparent opening and closing rate constants from open probabilities and activation/deactivation time constants using a modified Chen–Miller state diagram of channel activation (Chen & Miller, 1996; Chen & Chen, 2001; Duffield *et al.* 2003; Hebeisen & Fahlke, 2005). Because the maximum absolute open probabilities of WT and H573X hClC-2 channels are below 1, we cannot independently determine the absolute open probabilities

for the fast and slow gates. We therefore assumed that the fast and slow gates exhibit identical maximum open probabilities that are equal to the square root of the maximum open probability. In the calculation of the opening rate constants, this assumption introduces a maximum of 15% error. Closing rate constants can reliably be determined only for the fast gate and only at positive potentials at which the fast gate exhibits an open probability of 0.

In WT channels, the opening rate constants for the fast and slow gates exhibit similar voltage dependences (Figs 4F, G). H573X causes a fivefold increase of the fast and slow opening rate constants (Fig. 4F and G). The voltage dependence of fast opening rates is unaffected, while slow activation rate constants are slightly less voltage dependent in H573X channels than in WT (Table 1). The H573X truncation also increases and changes the voltage dependence of the fast closing rate constants of hClC-2 at positive potentials (Fig. 4H).

A single carboxy-terminus in a dimeric channel is sufficient to decelerate slow gating but not to set normal fast gating rates

Biochemical experiments reveal an association between the two carboxy-termini in ClC-0, ClC-Ka and ClC-5 (Meyer & Dutzler, 2006; Markovic & Dutzler, 2007; Meyer *et al.* 2007).

To examine the functional impact of a possible association of carboxy-termini in hClC-2, we engineered a hetero-concatameric WT–573X hClC-2 construct (Fig. 5A) in which a covalent linker connects the carboxy-terminus of WT hClC-2 to the amino-terminus of H573X hClC-2. Such a covalent link might impair movements of the carboxy-terminus and thus modify certain gating steps. To test for such a possibility, we constructed a WT–WT concatamer and compared concatameric channels with channels expressed after transfection of the monomeric construct. No differences were observed in voltage dependences of the relative open probabilities and time constants of fast and slow gates (Supplementary Fig. 2). Expression levels of WT–WT concatamers were rather low (late current amplitude at -155 mV: -0.83 ± 0.27 nA, $n = 6$), preventing the accurate determination of the slow deactivation time constant at positive potentials. We could therefore not compare slow deactivation time constants for monomeric and concatameric WT channels. We also designed and expressed a heteroconcatamer in the inverse orders (H573X–WT). WT–H573X and H573X–WT heteroconcatamers display similar fast and slow gating (Supplementary Fig. 2). We conclude that linker sequence does not cause major alterations of hClC-2 gating, as reported for corresponding constructs of ClC-0

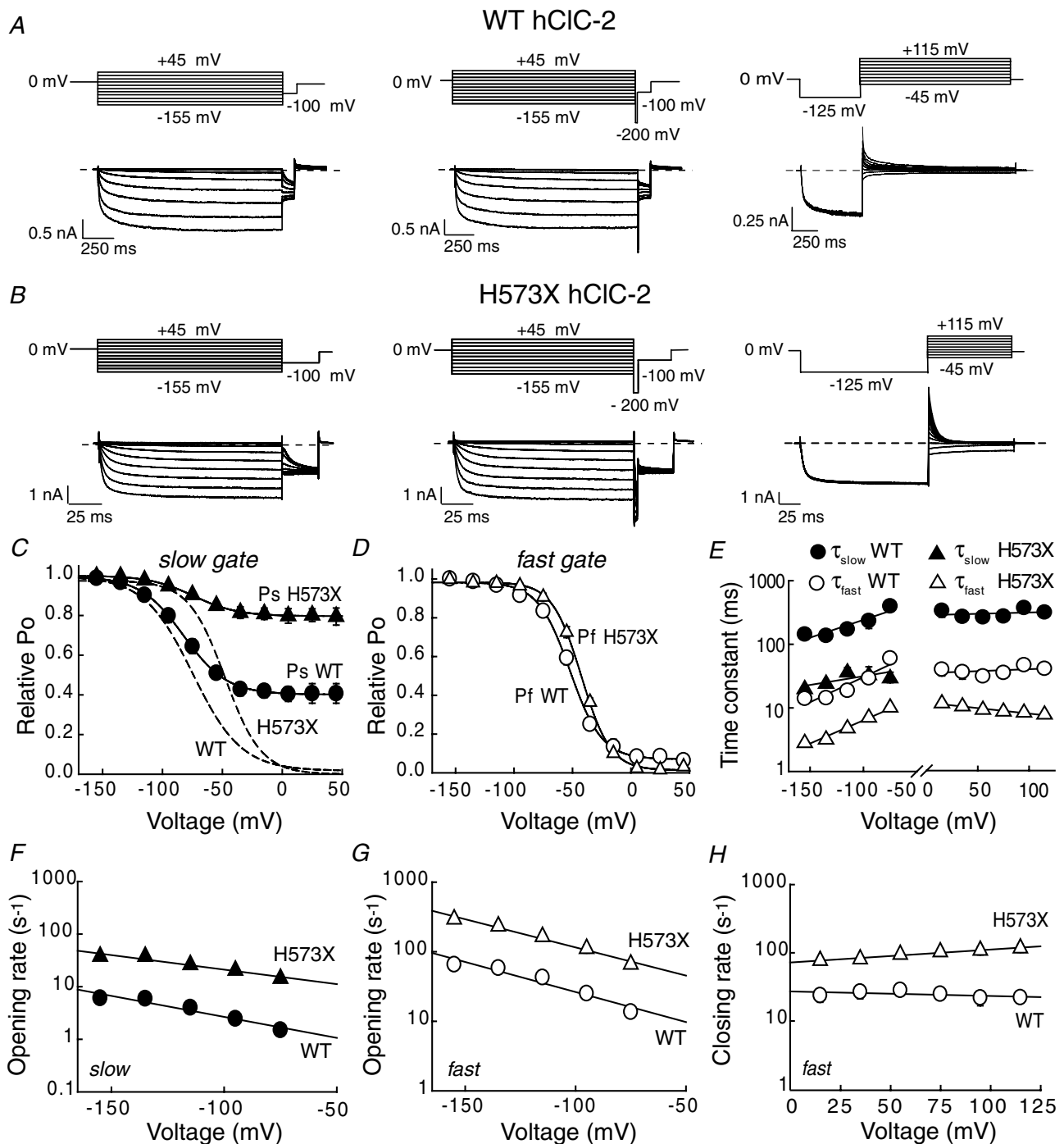


Figure 4. Complete removal of the carboxy-terminus modifies the fast and slow gating of hCIC-2

A and *B*, representative current traces and pulse protocols used to calculate the relative open probability (P_o , left panel), the open probability of the slow gate (P_s , middle panel), and the time course of deactivation (right panel) of WT (*A*) and H573X (*B*) channels. *C*, voltage dependences of the slow gate open probabilities (P_s) of WT ($n = 7$) and H573X ($n = 5$) channels. Continuous lines give fits to Boltzmann functions. Relative apparent open probabilities of WT and H573X hCIC-2 are shown as dashed lines. *D*, voltage dependences of the open probabilities of the fast gate (P_f) of WT ($n = 7$) and H573X hCIC-2 ($n = 5$). *E*, voltage dependences of the fast and slow activation and deactivation time constants of WT ($n = 10$) and H573X hCIC-2 ($n = 7$). *F–H*, voltage dependence of the fast opening rate constants (*F*), slow opening rate constants (*G*), and fast closing rate constants (*H*) for WT ($n = 5$) and H573X hCIC2 ($n = 4$) channels. Lines give fits to exponential functions (*E–H*).

Table 1. Voltage dependences of the opening (α) and closing rates (β) constants

	n	Opening				Closing	
		z	$\alpha_{\text{slow}} (-155 \text{ mV}) (\text{s}^{-1})$	z	$\alpha_{\text{fast}} (-155 \text{ mV}) (\text{s}^{-1})$	z	$\beta_{\text{fast}} (+115 \text{ mV}) (\text{s}^{-1})$
WT	4	0.20	6.1 ± 0.4	0.22	69.6 ± 5.4	0.02	22.2 ± 2.5
H573X	4	0.14	37.6 ± 0.8	0.20	293.5 ± 36.7	-0.05	117.0 ± 15.5
WT-H573X	4	0.07	8.6 ± 1.2	0.21	150.5 ± 33.1	-0.02	75.8 ± 8.7

(Ludewig *et al.* 1996), CIC-1 (Fahlke *et al.* 1997) and rCIC-2 (Weinreich & Jentsch, 2001).

Expression of the hetero-concatameric construct yielded channels with gating properties different from

WT and H573X homodimeric channels (Fig. 5B and C). At negative potentials, the fast time constants are smaller than those of WT and larger than those of H573X hCIC-2 channels, whereas slow time constants are similar to

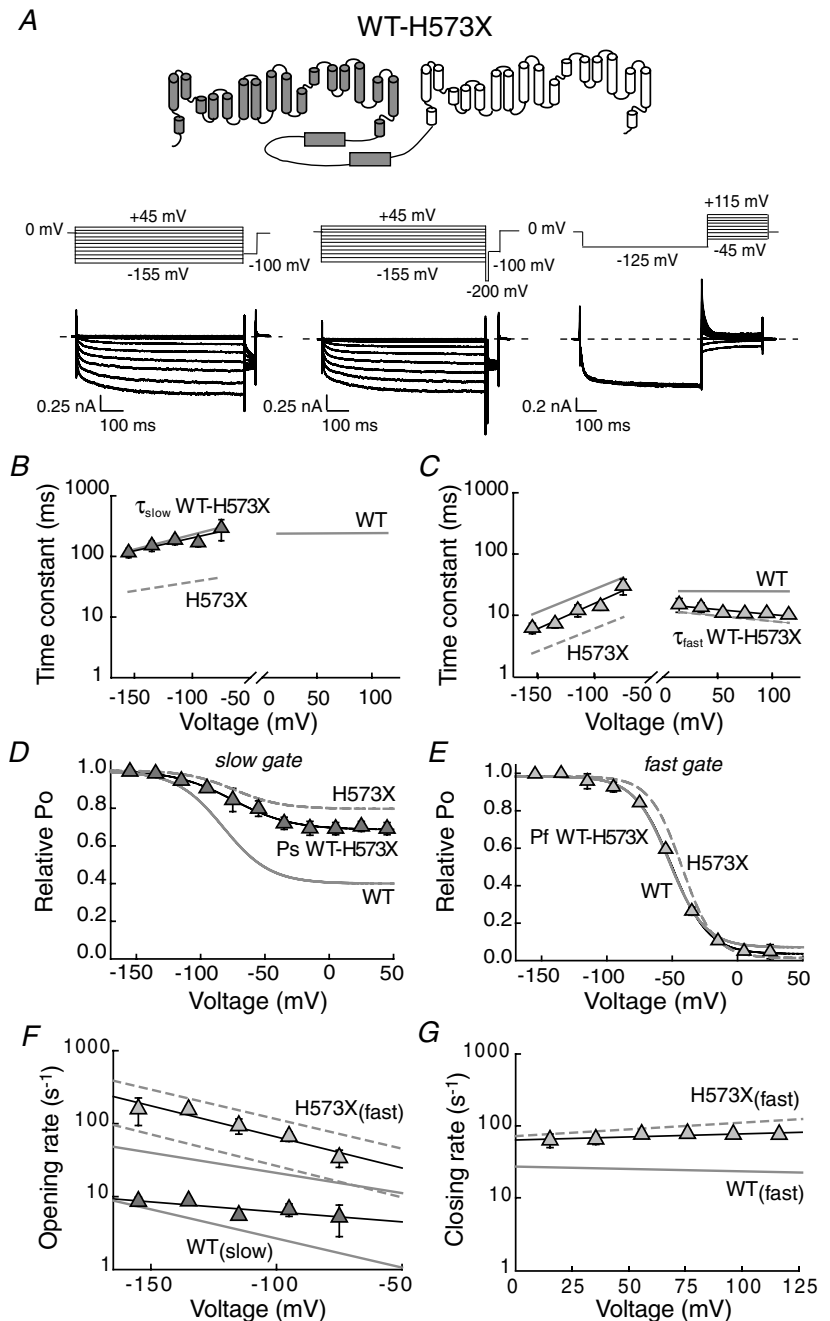


Figure 5. Properties of heterodimeric channels with only one complete carboxy-terminus

A, topology model, pulse protocols and representative whole-cell current traces of WT-H573X hetero-concatameric channels. B and C, voltage dependences of the slow (B) and fast (C) activation and deactivation time constants of WT-H573X hetero-concatamer ($n = 5$). Grey lines represent linear regressions to time constants of WT and H573X hCIC-2 from Fig. 4. D and E, voltage dependence of relative open probabilities of the slow (D, P_{s}) and the fast (E, P_{f}) gate of WT-H573X hCIC-2 hetero-concatamer ($n = 4$). Grey lines represent Boltzmann fits of P_{s} and P_{f} for WT and H573X channels shown in Fig. 4. C-F, voltage dependence of the fast and slow opening rate constants at negative potentials. G, voltage dependence of fast closing rate constants at positive potentials. Lines give fits to exponential functions (F and G).

the WT channels. Deactivation at positive potentials is monoexponential with time constants that completely superimpose fast time constants of homodimeric H573X channels. Thus, the contribution of homodimeric WT or mutant channels is negligible, and expression of the hetero-concatamer results in a preferential formation of heterodimeric channels with only one carboxy-terminus.

The minimum slow gate open probability (P_s) of heterodimers is intermediate to WT and H573X (WT–H573X: 0.68 ± 0.01 , $n = 5$) (Fig. 5D). Stationary noise analysis determined unitary currents and absolute open probabilities of heterodimeric channels similar to WT and H573X channels (data not shown). Slow activation time constants of heterodimeric channels do not differ from WT homodimeric channels, whereas open probabilities of the slow gate are increased in heterodimeric channels (Fig. 5B and D). Open probabilities of the fast gate (P_f) of heterodimeric channels with only one carboxy-terminus are very similar to homodimeric WT channels. In contrast, fast activation time constants of heterodimeric channels are close to the geometric mean of homodimeric WT and homodimeric truncated channels (Fig. 5C and E). Heterodimeric channels were completely blocked by 1 mM Cd^{2+} (Supplementary Fig. 1). A comparison of the relative block of WT and H573X homodimers and H573X–WT heterodimers by 100 μM Cd^{2+} demonstrates intermediate Cd^{2+} affinity for heterodimeric channels.

We next determined opening and closing rate constants for fast and slow gates. The voltage dependences of both rate constants of heterodimeric channels differ from those of homodimeric channels (Fig. 5F and G and Table 1). Slow opening rate constants of the WT–H573X heterodimeric channels are similar to those of WT at hyperpolarized potentials (Fig. 5F). We observed only one fast activation/deactivation time constant, indicating an adjustment of protopore gating within a heterodimeric channel. In the framework of the two-state model used in this study, this indicates that both protopores exhibit fast opening rate constants that are intermediate to WT and H573X homodimeric channels (Fig. 5F). All together, these results show that a single carboxy-terminus in a dimeric channel is sufficient to decelerate slow gating to WT values, whereas both carboxy-termini are necessary for normal fast gating.

Discussion

Mammalian ClC channels and transporters exhibit large carboxy-terminal cytoplasmic domains that fulfil diverse functions in separate isoforms. We here demonstrate that the main role of the carboxy-terminus of ClC-2 is modulation of channel gating. WT ClC-2 channels with full length carboxy-terminus activate on a slower time course than truncated channels. Removal of the

carboxy-terminal fragment distal to CBS2 results in faster activation and deactivation gating, and removal of the complete carboxy-terminus accelerates gating even further. In contrast, channels with only one CBS domain are permanently closed and can be opened by a point mutation (E205Q) that affects fast and slow gating (Zuniga *et al.* 2004; de Santiago *et al.* 2005).

The molecular mechanisms by which the carboxy-terminus modifies channel function are different in ClC-2 than in other ClC isoforms (Hryciw *et al.* 1998; Estevez *et al.* 2004; Hebeisen *et al.* 2004; Hebeisen & Fahlke, 2005). For ClC-1, complete removal of the carboxy-terminus results in a loss of function (Hebeisen *et al.* 2004) and an impaired surface membrane insertion of this isoform (Estevez *et al.* 2004). However, a single CBS domain is sufficient to preserve functional expression and normal gating (Estevez *et al.* 2004; Hebeisen *et al.* 2004; Wu *et al.* 2006), indicating that CBS domains are capable of functioning independently of each other in ClC-1. Whereas an incomplete CBS1–CBS2 pair permanently closes the channel (Fig. 2), hClC-2 is fully functional without its carboxy-terminus (Fig. 1). Since it is likely that $\text{CT}_{\text{hClC-2}}$ shares the same overall structure solved for other isoforms, this result implies that the carboxy-terminus interacts in a different way with gates that are activated by membrane depolarization in ClC-1, or by membrane hyperpolarization in ClC-2.

Cd^{2+} blocks ClC channels by facilitating common gating (Chen, 1998), and a comparison of the effect of Cd^{2+} on WT and truncated ClC-2 channels allows testing whether there are common gating processes in truncated channels. WT and H573X homodimeric as well as H573X–WT heterodimeric channels are completely blocked by 1 mM Cd^{2+} (Supplementary Fig. 1). Additional support for the idea that common gating is not abolished by carboxy-terminal truncation comes from the different degree of block by homodimeric and heterodimeric channels (Supplementary Fig. 1). Divalent cations bind with higher affinity to channels with closed common gates than to channels with open common gate (Chen, 1998). H573X hClC-2 exhibits larger open probabilities of the slow gate than WT and WT–H573X channels (Fig. 4) and displays the least pronounced block by 100 μM Cd^{2+} .

The carboxy-terminus of ClC-0 and ClC-1 channels is currently believed to play a crucial role in cooperative slow gating steps. Mutations in the carboxy-terminus affect voltage dependence and the time course of slow gating of ClC-0 and ClC-1 (Beck *et al.* 1996; Fong *et al.* 1998; Estevez *et al.* 2004). Furthermore, spectroscopic microscopy experiments demonstrated that slow gating of ClC-0 is associated with large movements of the carboxy-terminus. These movements were predicted to be transmitted to the transmembrane core resulting in cooperative closure of both protopores (Bykova *et al.* 2006). We here demonstrate that hClC-2 channels

lacking their complete carboxy-termini (H573X hClC-2) exhibit slow gating, albeit with faster opening and closing rate constants than WT. In heterodimeric WT–H573X channels, slow activation time constants are close to WT values, indicating that a single carboxy-terminus suffices to decelerate slow opening (Fig. 5). We conclude that the concerted action of slow gating is not conferred by intermolecular interactions between both carboxy-termini in hClC-2. This might be due to isoform-specific differences in slow gating. hClC-2 also differs from ClC-0 in a less pronounced temperature dependence of the slow gate of hClC-2 (Zuniga *et al.* 2004) as for ClC-0 (Pusch *et al.* 1997).

The effects of two carboxy-termini on fast gating are additive, suggesting that interactions between the two carboxy-termini are not necessary for modification of fast gating. The kinetics of the fast gates of H573X and WT hClC-2 are very different in homodimeric assemblies. However, only one fast deactivation component is observed in WT–H573X heterodimeric channels. Although hClC-2 gating might be more complicated than the kinetic model we used to determine opening and closing rate constants (Fig. 5), our results demonstrate that the WT protopore gates faster and the H573X protopore slower within a heterodimeric assembly than within a homodimer (Fig. 5). We conclude that each carboxy-terminus regulates both protopores.

Since mutant channels without the carboxy-terminus are functional and even activate much faster, the main physiological role of the ClC-2 carboxy-terminus appears to be slowing down activation and deactivation kinetics. Such a physiological role is unusual and at first glance surprising, yet it agrees well with a recently proposed physiological function of ClC-2 (Staley *et al.* 1996; Haug *et al.* 2003; Saint-Martin *et al.* 2008). ClC-2 opens only at a voltage negative to the chloride equilibrium potential, E_{Cl} (for example, when $[\text{Cl}^-]_i$ is increased after intense GABAergic inhibition). After opening, Cl^- ions move out of the cell until E_{Cl} approaches the resting membrane potential. Since the efflux of negative ions depolarizes the membrane, a fast activation of ClC-2 could potentially cause a rapid cell depolarization and recurrent action potential initiation. The carboxy-terminus may stabilize neuronal excitability by slowing down the fast and slow activation of ClC-2.

References

- Arreola J, Begenisich T & Melvin JE (2002). Conformation-dependent regulation of inward rectifier chloride channel gating by extracellular protons. *J Physiol* **541**, 103–112.
- Beck CL, Fahlke Ch & George AL Jr (1996). Molecular basis for decreased muscle chloride conductance in the myotonic goat. *Proc Natl Acad Sci U S A* **93**, 11248–11252.
- Bykova EA, Zhang XD, Chen TY & Zheng J (2006). Large movement in the C terminus of ClC-0 chloride channel during slow gating. *Nat Struct Mol Biol* **13**, 1115–1119.
- Carr G, Simmons N & Sayer J (2003). A role for CBS domain 2 in trafficking of chloride channel ClC-5. *Biochem Biophys Res Commun* **310**, 600–605.
- Catalan M, Niemyer ML, Cid LP & Sepulveda FV (2004). Basolateral ClC-2 chloride channels in surface colon epithelium: regulation by a direct effect of intracellular chloride. *Gastroenterology* **126**, 1104–1114.
- Chen TY (1998). Extracellular zinc ion inhibits ClC-0 chloride channels by facilitating slow gating. *J Gen Physiol* **112**, 715–726.
- Chen MF & Chen T (2001). Different fast-gate regulation by external Cl^- and H^+ of the muscle-type ClC chloride channels. *J Gen Physiol* **118**, 23–32.
- Chen TY & Miller C (1996). Nonequilibrium gating and voltage dependence of the ClC-0 Cl^- channel. *J Gen Physiol* **108**, 237–250.
- Cid LP, Montrose-Rafizadeh C, Smith DI, Guggino WB & Cutting GR (1995). Cloning of a putative human voltage-gated chloride channel (ClC-2) cDNA widely expressed in human tissues. *Hum Mol Genet* **4**, 407–413.
- de Santiago JA, Nehrke K & Arreola J (2005). Quantitative analysis of the voltage-dependent gating of mouse parotid ClC-2 chloride channel. *J Gen Physiol* **126**, 591–603.
- Duffield M, Rychkov GY, Bretag AH & Roberts ML (2003). Involvement of helices at the dimer interface in ClC-1 common gating. *J Gen Physiol* **121**, 149–161.
- Dutzler R, Campbell ED & MacKinnon R (2003). Gating the selectivity filter in ClC chloride channels. *Science* **300**, 108–112.
- Estevez R, Pusch M, Ferrer-Costa C, Orozco M & Jentsch TJ (2004). Functional and structural conservation of CBS domains from ClC chloride channels. *J Physiol* **557**, 363–378.
- Fahlke Ch, Knittle TJ, Gurnett CA, Campbell KP & George AL Jr (1997). Subunit stoichiometry of human muscle chloride channels. *J Gen Physiol* **109**, 93–104.
- Fong PY, Rehfeldt A & Jentsch TJ (1998). Determinants of slow gating in ClC-0, the voltage-gated chloride channel of *Torpedo marmorata*. *Am J Physiol Cell Physiol* **274**, C966–C973.
- Haug K, Warnstedt M, Alekov A, Sander T, Ramirez A, Poser B, Maljevic S, Hebeisen S, Kubisch C, Rebstock J, Horvath S, Hallmann K, Dullinger J, Rau B, Haverkamp F, Beyenbrug S, Schulz H, Janz D, Giese B, Müller-Newen G, Propping P, Elger C, Fahlke Ch, Lerche H & Heils A (2003). Mutations in the voltage-gated chloride channel ClC-2 are associated with idiopathic generalized epilepsies. *Nat Genet* **33**, 527–532.
- Hebeisen S, Biela A, Giese B, Müller-Newen G, Hidalgo P & Fahlke Ch (2004). The role of the carboxyl terminus in ClC chloride channel function. *J Biol Chem* **279**, 13140–13147.
- Hebeisen S & Fahlke Ch (2005). Carboxy-terminal truncations modify the outer pore vestibule of muscle chloride channels. *Biophys J* **89**, 1710–1720.
- Hebeisen S, Heidtmann L, Cosmelli D, Gonzalez C, Poser B, Latorre R, Alvarez O & Fahlke Ch (2003). Anion permeation in human ClC-4 channels. *Biophys J* **84**, 2306–2318.

- Hryciw DH, Rychkov GY, Hughes BP & Bretag AH (1998). Relevance of the D13 region to the function of the skeletal muscle chloride channel, ClC-1. *J Biol Chem* **273**, 4304–4307.
- Jentsch TJ, Stein V, Weinreich F & Zdebik AA (2002). Molecular structure and physiological function of chloride channels. *Physiol Rev* **82**, 503–568.
- Lin YW, Lin CW & Chen TY (1999). Elimination of the slow gating of ClC-0 chloride channel by a point mutation. *J Gen Physiol* **114**, 1–12.
- Ludewig U, Pusch M & Jentsch TJ (1996). Two physically distinct pores in the dimeric ClC-0 chloride channel. *Nature* **383**, 340–343.
- Maduke M, Williams C & Miller C (1998). Formation of ClC-0 chloride channels from separated transmembrane and cytoplasmic domains. *Biochemistry* **37**, 1315–1321.
- Markovic S & Dutzler R (2007). The structure of the cytoplasmic domain of the chloride channel ClC-Ka reveals a conserved interaction interface. *Structure* **15**, 715–725.
- Melzer N, Torres-Salazar D & Fahlke Ch (2005). A dynamic switch between inhibitory and excitatory currents in a neuronal glutamate transporter. *Proc Natl Acad Sci U S A* **102**, 19214–19218.
- Meyer S & Dutzler R (2006). Crystal structure of the cytoplasmic domain of the chloride channel ClC. *Structure* **14**, 299–307.
- Meyer S, Savaresi S, Forster IC & Dutzler R (2007). Nucleotide recognition by the cytoplasmic domain of the human chloride transporter ClC-5. *Nat Struct Mol Biol* **14**, 60–67.
- Mo L, Xiong W, Qian T, Sun H & Wills NK (2004). Coexpression of complementary fragments of ClC-5 and restoration of chloride channel function in a Dent's disease mutation. *Am J Physiol Cell Physiol* **286**, C79–C89.
- Niemeyer MI, Cid LP, Zuniga L, Catalan M & Sepulveda FV (2003). A conserved pore-lining glutamate as a voltage- and chloride-dependent gate in the ClC-2 chloride channel. *J Physiol* **553**, 873–879.
- Park K, Arreola J, Begeisich T & Melvin JE (1998). Comparison of voltage-activated Cl⁻ channels in rat parotid acinar cells with ClC-2 in a mammalian expression system. *J Membr Biol* **163**, 87–95.
- Pusch M, Ludewig U & Jentsch TJ (1997). Temperature dependence of fast and slow gating relaxations of ClC-0 chloride channels. *J Gen Physiol* **109**, 105–116.
- Pusch M, Ludewig U, Rehfeldt A & Jentsch TJ (1995). Gating of the voltage-dependent chloride channel ClC-0 by the permeant anion. *Nature* **373**, 527–530.
- Ramjeesingh M, Li C, She YM & Bear CE (2006). Evaluation of the membrane-spanning domain of ClC-2. *Biochem J* **396**, 449–460.
- Rychkov GY, Pusch M, Astill DSJ, Roberts ML, Jentsch TJ & Bretag AH (1996). Concentration and pH dependence of skeletal muscle chloride channel ClC-1. *J Physiol* **497**, 423–435.
- Saint-Martin C, Gauvain G, Teodorescu G, Gourfinkel-An I, Fedirko E, Weber YG, Maljevic S, Ernst JP, Garcia-Olivares J, Fahlke Ch, Nabbout R, LeGuern E, Lerche H, Poncer JC & Depienne C (2008). Two novel *CLCN2* mutations accelerating Cl⁻ channel deactivation are associated with idiopathic generalized epilepsy. *Hum Mutat* (in press).
- Schwappach B, Stobrawa S, Hechenberger M, Steinmeyer K & Jentsch TJ (1998). Golgi localization and functionally important domains in the NH₂ and COOH terminus of the yeast ClC putative chloride channel Gef1p. *J Biol Chem* **273**, 15110–15118.
- Sesti F & Goldstein SAN (1998). Single-channel characteristics of wild-type IKs channels and channels formed with two minK mutants that cause long QT syndrome. *J Gen Physiol* **112**, 651–663.
- Sigworth FJ (1980). The variance of sodium current fluctuations at the node of Ranvier. *J Physiol* **307**, 97–129.
- Staley K, Smith R, Schaack J, Wilcox C & Jentsch TJ (1996). Alteration of GABA_A receptor function following gene transfer of the ClC-2 chloride channel. *Neuron* **17**, 543–551.
- Thiemann A, Gründer S, Pusch M & Jentsch TJ (1992). A chloride channel widely expressed in epithelial and non-epithelial cells. *Nature* **356**, 57–60.
- Torres-Salazar D & Fahlke Ch (2007). Neuronal glutamate transporters vary in substrate transport rate but not in unitary anion channel conductance. *J Biol Chem* **282**, 34719–34726.
- Weinreich F & Jentsch TJ (2001). Pores formed by single subunits in mixed dimers of different ClC chloride channels. *J Biol Chem* **276**, 2347–2353.
- Wu W, Rychkov GY, Hughes BP & Bretag AH (2006). Functional complementation of truncated human skeletal-muscle chloride channel (hClC-1) using carboxyl tail fragments. *Biochem J* **395**, 89–97.
- Zuniga L, Niemeyer MI, Varela D, Catalan M, Cid LP & Sepulveda FV (2004). The voltage-dependent ClC-2 chloride channel has a dual gating mechanism. *J Physiol* **555**, 671–682.

Acknowledgements

We would like to thank Dr. Simon Hebeisen and Dr. Delany Torres-Salazar for helpful discussions; Dr. Rudolf Bauerfeind for help with the confocal microscopy; and Dr. Gary Cutting for providing the human ClC-2 cDNA. J. Garcia-Olivares was a student from the Facultad de Ciencias, Universidad de Chile, and was supported by the Beca Integrada programme of the Deutscher Akademischer Austauschdienst. These studies were supported by the Deutsche Forschungsgemeinschaft.

Supplemental material

Online supplemental material for this paper can be accessed at: <http://jp.physoc.org/cgi/content/full/jphysiol.2008.158097/DC1>